ALD TiO$_2$ thin film as dielectric for Al/p-Si Schottky diode

SEFA B K AYDIN[a], DİLBER E YILDIZ[b], HATİCE KANBUR ÇAVUŞ[a,*] and RECEP ŞAHİNGÖZ[a]

[a]Department of Physics, Faculty of Arts and Sciences, Bozok University, Yozgat 66100, Turkey
[b]Department of Physics, Faculty of Arts and Sciences, Hitit University, Çorum 19030, Turkey

Abstract. Electrical analysis of Al/p-Si Schottky diode with titanium dioxide (TiO$_2$) thin film was performed at room temperature. The forward and reverse bias current–voltage (*I–V*) characteristics of diode were studied. Using thermionic emission (TE) theory, the main electrical parameters of the Al/TiO$_2$/p-Si Schottky diode such as ideality factor (*n*), zero bias barrier height (ϕ_{Bo}) and series resistance (R_s) were estimated from forward bias *I–V* plots. At the same time, values of *n*, ϕ_{Bo} and R_s were obtained from Cheung's method. It was shown that electrical parameters obtained from TE theory and Cheung's method exhibit close agreement with each other. The reverse-bias leakage current mechanism of Al/TiO$_2$/p-Si Schottky barrier diodes was investigated. The *I–V* curves in the reverse direction are taken and interpreted via both Schottky and Poole–Frenkel effects. Schottky effect was found to be dominant in the reverse direction. In addition, the capacitance–voltage (*C–V*) and conductance–voltage (*G/w–V*) characteristics of diode were investigated at different frequencies (50–500 kHz). The frequency dependence of interface states density was obtained from the Hill–Coleman method and the voltage dependence of interface states density was obtained from the high–low frequency capacitance method.

Keywords. ALD TiO$_2$; electrical properties; interface state density; Schottky effect; Poole–Frenkel emission.

1. Introduction

Recently, titanium dioxide (TiO$_2$) has great importance because of its high dielectric constant, high thermal stability, large band gap, high refractive index and low leakage current density. It has potential applications such as catalysis, sensors, antireflection coating, solar cells and Schottky diodes (Kadoshima *et al* 2003; Pakma *et al* 2008, 2009, 2011; Kınacı *et al* 2012; Landmann *et al* 2012; Nasim *et al* 2012; Rathee *et al* 2012; Sekhar *et al* 2012; Sönmezoğlu and Akın 2012). TiO$_2$ are fabricated by various techniques such as chemical vapor deposition, electron beam evaporation, the sol–gel method, sputtering, atomic layer deposition (ALD) method, etc. Among them, the ALD technique has been employed to grow ultra-thin and high-*k* dielectrics on a substrate owing to its advantages over other deposition methods such as excellent thickness uniformity over large substrate areas, low processing temperature, low impurity content and completely precise thickness control (Lu *et al* 2006; Xuan *et al* 2006; Shahrjerdi *et al* 2007; Wu *et al* 2007; Hoogeland *et al* 2009).

Metal–semiconductor (MS) and metal–insulator–semiconductor (MIS) Schottky diodes have an important role in the integrated device technology (Pakma *et al* 2008, 2009, 2011; Kınacı *et al* 2012; Sönmezoğlu and Akın 2012). The current-transport mechanisms in these devices are dependent on a variety of factors such as fabrication parameters of semiconductors, formation of insulator layer, device

temperature and bias voltage, etc. There are various models such as thermionic emission (TE), thermionic field emission (TFE), recombination generation, multistep tunneling compete, Poole–Frenkel and space charge limited-conduction (SCLC) mechanisms to explain charge transport mechanisms and generally, one of them may dominate. However, two and more mechanisms could be used together at certain special conditions. But a complete description of conduction mechanisms through Schottky contact is still a challenging problem. Therefore, the analysis of forward and reverse current mechanisms is important.

In this paper, we have investigated characteristics of *I–V*, *C–V* and *G/w–V* of Al/TiO$_2$/p-Si Schottky diode. We have discussed the reverse and forward current conduction mechanisms of Al/TiO$_2$/p-Si Schottky diode and Schottky diode parameters such as ϕ_{Bo}, *n*, R_s and N_{ss} are determined.

2. Experimental

Al/TiO$_2$/p-Si Schottky diodes used were fabricated using p-type (boron-doped) single-crystal silicon wafer with $\langle 111 \rangle$ surface orientation, having a thickness of 300 μm and a resistivity of 5–10 Ω cm. For the fabrication process, the Si wafer was degreased in an organic solvent of CHClCCl$_2$, CH$_3$COCH$_3$ and CH$_3$OH; etched in a sequence of H$_2$SO$_4$ and H$_2$O$_2$, 20% HF and a solution of 6HNO$_3$:1HF:35H$_2$O, 20% HF; and finally quenched in de-ionized water with a resistivity of 18 MΩ cm for a prolonged time. High purity (99·999%) aluminum (Al) with a thickness of 2000 Å was

thermally evaporated from the tungsten filament onto the whole backside of half of a wafer at a pressure of $\sim 10^{-6}$ Torr. Low-resistance ohmic contacts were formed by thermal annealing at 400 °C for 5 min in flowing N_2 in a quartz tube furnace. After ohmic contact, a layer of TiO_2 was grown on the Si substrate by atomic layer deposition (ALD) technique (George *et al* 1994, 1996; Lu *et al* 2006; Xuan *et al* 2006; Shahrjerdi *et al* 2007; Wu *et al* 2007; Hoogeland *et al* 2009) by high-vacuum ALD Savannah S300 system. Immediately after TiO_2 growth on Si wafer, Al (99·999%) with a thickness of 2000 Å was thermally evaporated from the tungsten filament onto the TiO_2 surface through metal shadow masks with circular dots of ~ 2 mm diameter. Finally, Al/TiO_2/ p-Si Schottky contacts were formed. The energy level and schematic diagram of Al/TiO_2/p-Si Schottky diode are presented in figure 1(a) and (b), respectively. The metal thickness layer and deposition rates were monitored with the help of quartz crystal thickness monitor. The quartz crystal thickness monitor is used to record the metal thickness layer and deposition rates.

Albeit, ALD is a surface controlled layer-by-layer process for the deposition of thin film with atomic layer accuracy, we controlled TiO_2 thick with UCF Stylus Profilometer. The TiO_2 thick was measured at about 25 Å. The I–V, C–V and G/w–V characteristics of Al/TiO_2/p-Si diode was measured at room temperature by the Keithley 4200 UCF Semiconductor Parameter Analyzer.
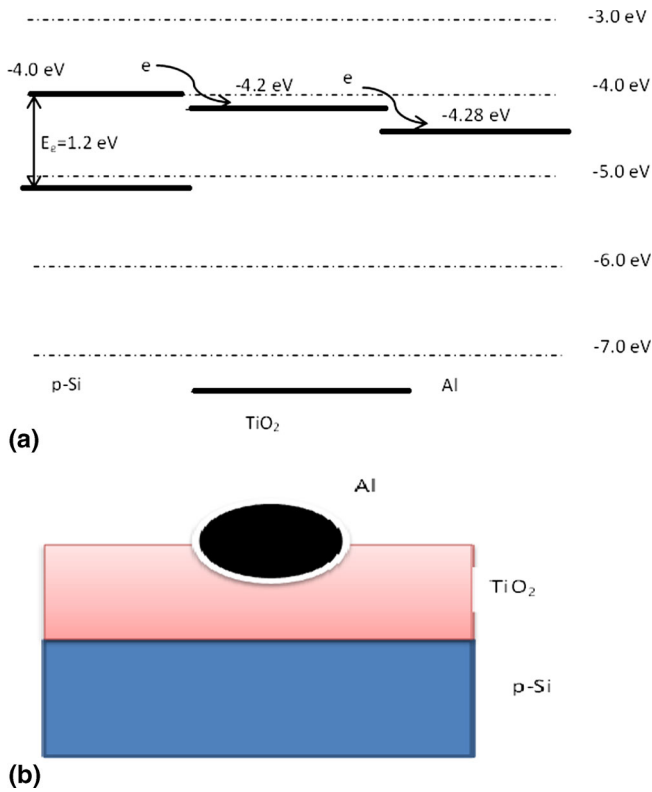
3. Results and discussion

3.1 *Forward and reverse bias I–V characteristics*

Figure 2 shows the experimental semi-log forward and reverse bias I–V characteristics of Al/TiO_2/p-Si Schottky diodes at room temperature. As can be seen in figure 2, Al/TiO_2/p-Si Schottky diode exhibits rectifying behaviour. In forward bias I–V characteristics of Schottky contacts, the relationship between the applied-bias voltage ($V \geq 3kT/q$) and the current according to thermionic emission (TE) theory is given by (Sze 1981; Rhoderick and Williams 1988; Güllü *et al* 2012; Reddy and Reddy 2012)

$$I = I_o \exp\left(\frac{q(V - IR_s)}{nkT}\right)\left[1 - \exp\left(-\frac{q(V - IR_s)}{kT}\right)\right],$$
(1a)

where q is the electronic charge, V the applied voltage, R_s the series resistance, n the ideality factor, k the Boltzmann constant and T the temperature in Kelvin. I_o is the saturation current and is determined by

$$I_o = A^* A T^2 \exp(-q\phi_{Bo}/kT),$$
(1b)

where A^*, A, ϕ_{Bo} are the effective Richardson constant (32A cm^{-2} K^{-2} for p-type Si) (Sze 1981; Rhoderick and Williams 1988), the area of rectifier contact, the zero-bias barrier height, respectively. The saturation current value I_o
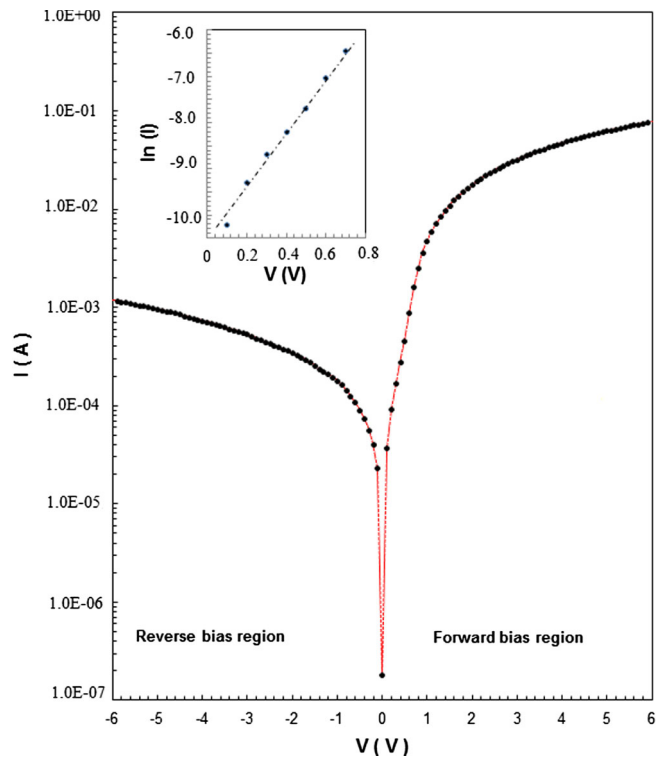

Figure 1. (**a**) Energy level diagram and (**b**) schematic diagram of Al/TiO_2/p-Si Schottky diode.

Figure 2. Semi-log current–voltage characteristics of Al/TiO_2/p-Si Schottky diode.

was found from the intercept of the linear portion of the forward bias semi-logarithmic $\ln(I) - V$ plot at zero bias. The term IR_s is the voltage drop across the series resistance of the diode.

The value of ideality factor (n) was determined by the linear region of the $\ln(I) - V$ plot (figure 2) and can be written as from (1a)

$$n = \frac{q}{kT}\left(\frac{\mathrm{d}(V - IR_s)}{\mathrm{d}(\ln(I))}\right). \tag{2}$$

The values of n and ϕ_{Bo} were obtained as 1·80 and 0·66 eV, respectively. Normally, it is $n = 1$ for an ideal state. Great value of the ideality factor has been attributed to particular distribution of interface states and TiO₂ insulator layer between metal and semiconductor (Card and Rhoderick 1971; Janardhanam *et al* 2012).

The downward bending at adequately high bias voltages was induced by the effect of R_s, apart from the existence of the interface states (Pakma *et al* 2009, 2011; Kınacı *et al* 2012). Therefore n, ϕ_{Bo} and R_s were calculated from the Cheung and Cheung (1986) method in the high current range. From (1a), the following functions can be expressed as

$$\frac{\mathrm{d}V}{\mathrm{d}(\ln I)} = n\frac{kT}{q} + R_s I, \tag{3}$$

$$H(I) = V - n\frac{kT}{q}\ln\left(\frac{I}{AA^*T^2}\right) = n\phi_B + R_s I, \tag{4}$$

where ϕ_B is the barrier height obtained from data of downward bending region in the forward bias $I–V$ plots. In figure 3, experimental $\mathrm{d}V/\mathrm{d}(\ln I)$ vs I and $H(I)$ vs I plots are presented for Al/TiO₂/p-Si Schottky diode. As can be given in figure 3, equations (3) and (4) should give a straight line for the data of downward bending region in the forward bias $I–V$ characteristic. Hence, a plot of $\mathrm{d}V/\mathrm{d}(\ln I)$ vs I will give R_s as the slope and nkT/q as the y-axis intercept. The $H(I)$ functions were derived by using these n values in (4). The plot of $H(I)$ vs I will also lead to a straight line (figure 3) with a y-axis intercept that is equal to $n\phi_B$. The
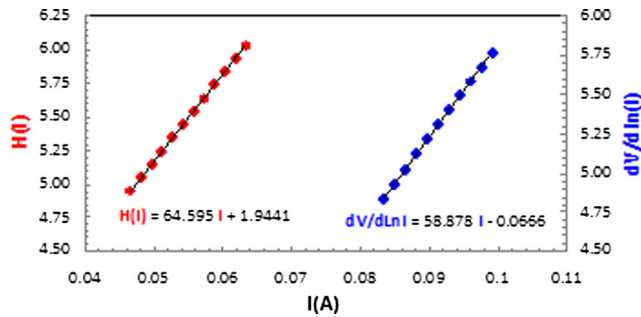
slope of $H(I)$ vs I plot also provides a second determination of R_s. As shown in table 1, the values of n and ϕ_B obtained from TE theory and Cheung methods are close to each other.

From figure 2, it is evident that the exponential dependence of reverse current (I_R) strongly suggests that Poole–Frenkel or Schottky barrier lowering mechanisms are operative in the junction. The reverse current–voltage expressions for Poole–Frenkel effect are given as (Soylu *et al* 2013)

$$J_R = J_o \exp\left(\frac{\beta_{PF}}{k_B T}\sqrt{E}\right) = I_o \exp\left(\frac{\beta_{PF}}{k_B T d^{1/2}}V^{1/2}\right)(E = V/d). \tag{5}$$

For the Schottky effect

$$J_R = A^*T^2 \exp(\phi_s/kT)\exp\left(\frac{\beta_S}{k_B T}\sqrt{E}\right)$$
$$= A^*T^2 \exp\left(\frac{\beta_S}{k_B T d^{1/2}}V^{1/2}\right), \tag{6}$$

where β_{PF} and β_S are the Poole–Frenkel and Schottky field-lowering coefficients, respectively.

$$\beta_{PF} = 2\beta_S = \left(\frac{q}{\pi \varepsilon_i}\right)^{1/2}. \tag{7}$$

Here, ε_i is the permittivity of insulator layer TiO₂ and $\varepsilon_i = 48\varepsilon_o$ (Lu *et al* 2006; Xuan *et al* 2006; Shahrjerdi *et al* 2007; Wu *et al* 2007; Hoogeland *et al* 2009) and ε_o is the permittivity of free space.

In principle, the Poole–Frenkel and Schottky effects can be distinguished by measured values of field-lowering coefficients (β_{PF}) is always twice the value of Schottky field coefficients (β_S). The theoretical values of these coefficients for Al/TiO₂/p-Si Schottky contact are $\beta_{PF} = 1·0 \times 10^{-4}$ eV/m$^{1/2}$ V$^{-1/2}$ and $\beta_S = 5·48 \times 10^{-5}$ eV/m$^{1/2}$ V$^{-1/2}$. Plots of $\ln(I_R)$ vs $E^{1/2}$ and $\ln(J_R/A^*T^2)$ vs $V^{1/2}$ for Al/TiO₂/p-Si Schottky contact at room temperature is shown in figure 4(a) and (b). The experimental value of β obtained from slope of linear region in figure 4(a) is $4·61 \times 10^{-5}$ eV/m$^{1/2}$ V$^{-1/2}$ for 300 K. In addition, the experimental value of β_S obtained from slope of linear region in figure 4(b) is $3·26 \times 10^{-5}$ eV/m$^{1/2}$ V$^{-1/2}$ for diode. The experimentally calculated value of β for diode is closer to the theoretical values of β_S and therefore Schottky effect is more dominated in reverse direction as the experimentally value of β is more close to theoretical Schottky coefficient.

Figure 3. Plots of the Al/TiO₂/p-Si Schottky diode $\mathrm{d}V/\mathrm{d}\ln(I)$ vs I and $H(I)$ vs I.

Table 1. Experimental values of parameters obtained from $I–V$ characteristics of Al/TiO₂/p-Si Schottky diode at room temperature.

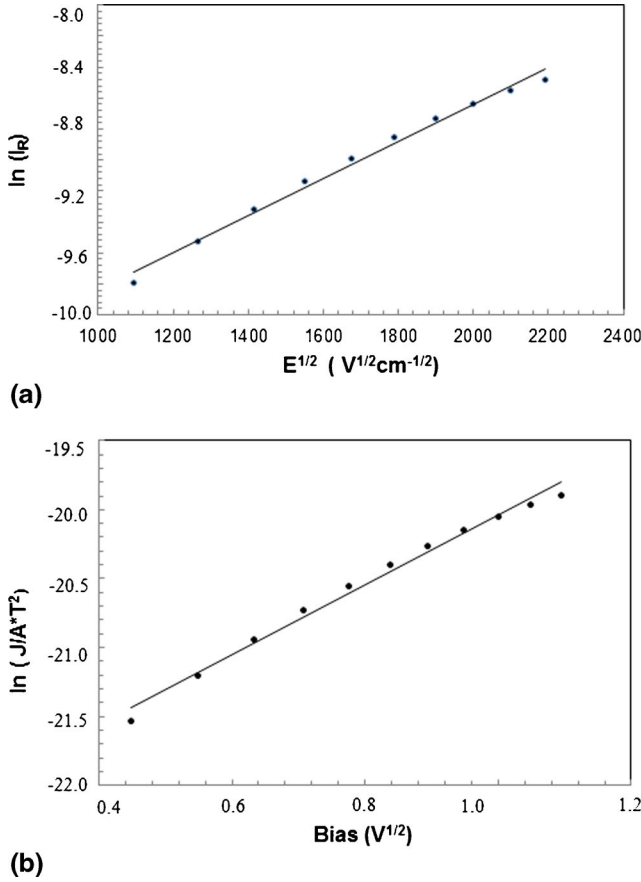|	I_o (A)	n	ϕ_{Bo} (eV)	R_s (Ω)
TE	$7·23 \times 10^{-7}$	2·96	0·66	–
$\mathrm{d}V/\mathrm{d}\ln(I)$	–	2·55	–	58·88
$H(I)$	–	–	0·76	64·60

Figure 4. (a) $\ln(I_R)$ vs $E^{1/2}$ plot and (b) $\ln(J_R/A^*T^2)$ vs $V^{1/2}$ plot for Al/TiO$_2$/p-Si Schottky diode.

Figure 5. (a) $C-V$ plots and (b) $G/w-V$ plots for Al/TiO$_2$/p-Si Schottky diode.

3.2 *Capacitance–voltage (C–V) and conductance–voltage (G/w–V) characteristics*

Variations of $C-V$ and $G/w-V$ measurements for Al/TiO$_2$/p-Si Schottky diode were performed at different frequencies (50–500 kHz). As can be seen in figure 5(a) and (b), the values of the capacitance and conductance at negative voltages do not change with frequency. However at positive voltages, the values of the capacitance and conductance show an important change with frequency. In figure 5, the values of capacitance give the peaks while conductance almost increases with increasing voltage. The frequency dependence of capacitance and conductance characteristics may be caused by the presence of Schottky barrier, unintentionally doped atoms, the series resistance and interface state density effect. The series resistance and surface states of the Schottky contact are responsible for an abnormal bias dependence of the capacitance and conductance (Sze 1981; Nicollian and Brews 1982; Rhoderick and Williams 1988). At the same time, the values of capacitance and conductance increase with decreasing frequencies because of the fact that at higher frequencies the N_{ss} cannot follow the ac signal.

The voltage- and frequency-dependent series resistance can be obtained by the data in figure 5(a) and (b) when the
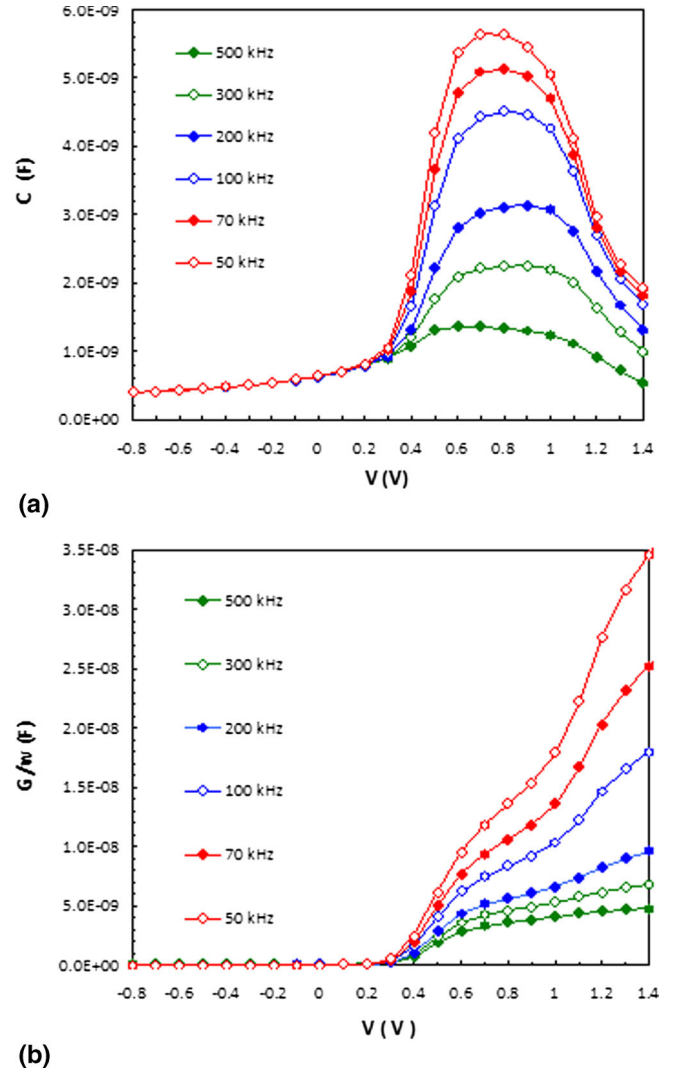
MIS structure is biased into strong accumulation, the admittance Y_{ma} is given by (Sze 1981; Nicollian and Brews 1982; Rhoderick and Williams 1988)

$$Y_{ma} = [G_m + jwC_m]. \tag{8}$$

Comparing the real and imaginary parts of admittance, the series resistance of MIS structure is expressed as (Sze 1981; Rhoderick and Williams 1988)

$$R_s = \frac{G_{ma}}{G_{ma}^2 + (\omega C_{ma})^2}, \tag{9}$$

where C_{ma} and G_{ma} represent the measured capacitance and conductance in the strong accumulation region.

In figure 6, the values of R_s give the peaks about positive bias where the interface states are intensive. The values of R_s are calculated from the measured capacitance C_{ma} and

conductance G_{ma} at strong accumulation and are given in table 2 for different frequencies.

The frequency dependence of interface states density was obtained from the $C-V$ and $G/w-V$ measurements by using the Hill–Coleman method (Hill and Coleman 1980). In this method, N_{ss} is given by

$$N_{ss} = \left(\frac{2}{qA}\right)\frac{(G_m/\omega)_{max}}{((G_m/\omega)_{max}C_{ox})^2 + (1 - C_{max}/C_{ox})^2},$$
(10)

where A is the area of the rectifier contact area of diode, ω the angular frequency, C_{max} and $(G_m/\omega)_{max}$ the measured C and G/w which correspond to peak values, respectively, and C_{ox} the capacitance of insulator layer. As can be seen from figure 7 and table 2, the values of N_{ss} were found to decrease with increasing frequencies. Such behavior of N_{ss} can be explained on the basis of assumption that only almost all of the interface states cannot follow the applied ac signal sufficiently high frequency (Sze 1981; Nicollian and Brews 1982; Rhoderick and Williams 1988).

The high–low frequency capacitance method is a practical method to obtain interface states density. In this method, the voltage dependence of interface states density was obtained from the high (for this study 500 kHz) and low (for this

study 50 kHz) $C-V$ measurements by using the following relationship (Yıldırım *et al* 2013):

$$N_{ss} = \frac{1}{qA}\left[\left(\frac{1}{C_{LF}} - \frac{1}{C_{ox}}\right)^{-1} - \left(\frac{1}{C_{HF}} - \frac{1}{C_{ox}}\right)^{-1}\right],$$
(11)

where C_{LF}, C_{HF}, and C_{ox} are the low frequency, high frequency, and oxide capacitance, respectively, q the electronic charge and A the rectifying contact area. In figure 8, the voltage dependence of interface states density is seen.
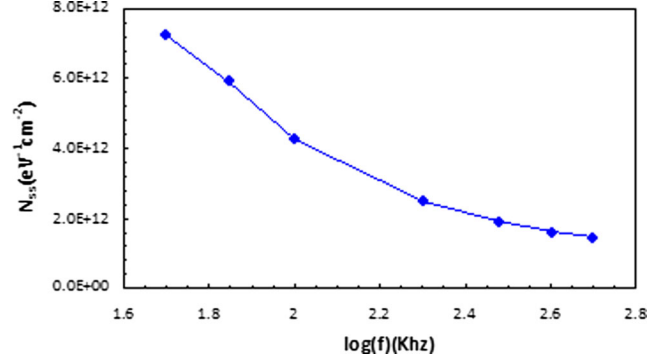

Figure 7. Variation of the interface states density for the Al/TiO$_2$/p-Si Schottky diode as a function of the frequency at room temperature.
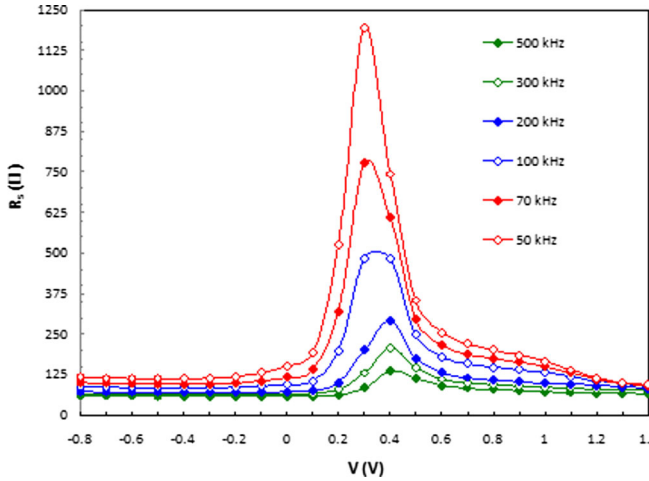

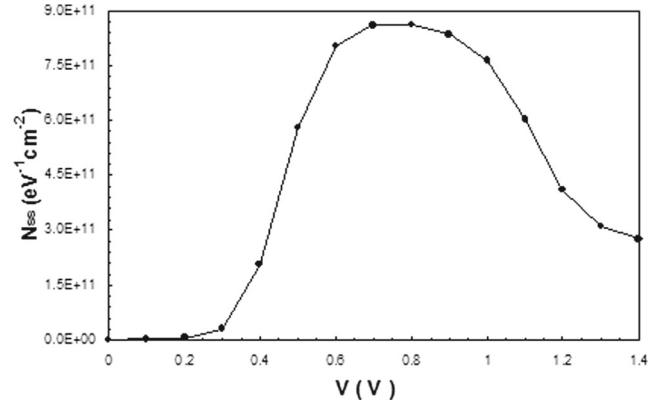**Figure 6.** R_s plots of Al/TiO$_2$/p-Si Schottky diode for different frequencies.

Figure 8. Interface states density versus voltage plot of Al/TiO**$_2$**/p-Si Schottky diode.

Table 2. Experimental values of parameters obtained from $C-V$ characteristics of Al/TiO$_2$/p-Si Schottky diode for different frequencies.

F (kHz)	V_{max} (V)	C_{max} (F)	G/w_{max} (F)	N_{ss} (cm^{-2}eV^{-1})	R_s (Ω)
500	0·6	$1·37 \times 10^{-9}$	$2·84 \times 10^{-9}$	$1·14 \times 10^{12}$	63·1
300	0·8	$2·25 \times 10^{-9}$	$4·58 \times 10^{-9}$	$1·84 \times 10^{12}$	73·6
200	0·8	$3·11 \times 10^{-9}$	$5·64 \times 10^{-9}$	$2·27 \times 10^{12}$	77·2
100	0·8	$4·51 \times 10^{-9}$	$8·35 \times 10^{-9}$	$3·38 \times 10^{12}$	82·1
70	0·8	$5·13 \times 10^{-9}$	$1·10 \times 10^{-9}$	$4·30 \times 10^{12}$	83·7
50	0·7	$5·65 \times 10^{-9}$	$1·18 \times 10^{-9}$	$4·81 \times 10^{12}$	85·4

4. Conclusions

The conduction mechanism and electronic parameters of Al/TiO$_2$/p-Si Schottky diode have been investigated by means of I–V, C–V and G/w–V measurements at room temperature. Using thermionic emission (TE) theory, n is found to be 1·8 and ϕ_{Bo} is found to be 0·66 eV. The high value of n may be explained on the basis of TE. The reverse bias current density was interpreted in terms of the two field lowering mechanisms, which are Poole–Frenkel and Schottky mechanism. It was seen that the conduction process can be best explained by Schottky effect in the reverse direction.

At the same time, C–V and G/w–V plots of Al/TiO$_2$/p-Si Schottky diode was analyzed for different frequencies (50–500 kHz). The forward bias C–V plots exhibited an anomalous peak. Such behavior is mainly attributed to the molecular restructuring and reordering of the N_{ss} and R_s. The values of N_{ss} of the Al/TiO$_2$/p-Si Schottky diode were performed by the Hill–Coleman and high–low frequency capacitance method.

Acknowledgements

References

Card H C and Rhoderick E H 1971 *J. Phys.* **D4** 1589

Cheung S K and Cheung N W 1986 *Appl. Phys. Lett.* **49** 85

George S, Sneh O, Dillon A C, Wise M L, Ott A W, Okada L A and Way J D 1994 *Appl. Surf. Sci.* **82/83** 460

George S M, Ott A W and Klaus J W 1996 *J. Phys. Chem.* **100** 13121

Güllü Ö, Aydoğan S and Türüt A 2012 *Thin Solid Films* **520** 1944

Hill W A and Coleman C C 1980 *Solid-State Electron.* **23** 987

Hoogeland D, Jinesh K B, Roozeboom F *et al* 2009 *J. Appl. Phys.* **106** 114107

Janardhanam V, Park Y K, Ahn K S and Choi C J 2012 *J. Alloys Compd.* **534** 37

Kadoshima M, Hiratani M, Shimamoto Y, Torii K, Miki H, Kimura S and Nabatame T 2003 *Thin Solid Films* **424** 224

Kınacı B, Çetin S Ş, Bengi A and Özçelik S 2012 *Mater. Sci. Semicond. Process* **15** 531

Landmann M, Rauls E and Schmidt W G 2012 *J. Phys. Condens. Matter* **24** 195503

Lu H L, Sun L Ding S J, Xu M, Zhang D W and Wang L K 2006 *Appl. Phys. Lett.* **89** 152910

Nasim F, Ali A, Hafizuddin M and Bhatti A S 2012 *J. Appl. Phys.* **112** 044513

Nicollian E H and Brews J R 1982 *MOS (metal/oxide/semiconductor) physics and technology* (New York: Wiley)

Pakma O, Serin N, Serin T and Altındal Ş 2008 *J. Appl. Phys.* **104** 014501

Pakma O, Serin N, Serin T and Altındal Ş 2009 *Sol-Gel Sci. Technol.* **50** 28

Pakma O, Serin N, Serin T and Altındal Ş 2011 *Physica B* **406** 771

Rathee D, Kumar M and Arya S K 2012 *Solid-State Electron.* **76** 71

Reddy N N K and Reddy V R 2012 *Bull. Mater. Sci.* **35** 53

Rhoderick E H and Williams R H 1988 *Metal semiconductor contacts* (Oxford: Clarendon) 2nd edn

Sekhar M C, Kondaiah P, Chandra S V J, Rao G M and Uthanna S 2012 *Surf. Interface Anal.* **44** 1299

Shahrjerdi D, Tutuc E and Banerjee S K 2007 *Appl. Phys. Lett.* **91** 063501

Sönmezoğlu S and Akın S 2012 *Curr. Appl. Phys.* **12** 1372

Soylu M, Al-Hartomy, Said S A F, Al-Ghamdi A A, Yahia I S and Yakuphanoglu F 2013 *Microelectron. Reliab.* **53** 1901

Sze S M 1981 *Physics semiconductor devices* (New York: John Wiley and Sons) 2nd edn

Wu Y Q, Shen T and Ye P D 2007 *Appl. Phys. Lett.* **90** 143504

Xuan Y, Ye P D and Lin H C 2006 *Appl. Phys. Lett.* **89** 132103

Yıldırım M, Durmuş P and Altındal Ş 2013 *Chin. Phys. B* **22** 108502